


Article

Water-Soluble Anions in PM₁₀ Samples Collected in the Metropolitan Area of Costa Rica: Temporal and Spatial Variations

Jorge Herrera-Murillo * , Tomas Soto-Murillo, José Félix Rojas-Marín, Victor Hugo Beita-Guerrero and María Hidalgo-Gutiérrez

Environmental Analysis Laboratory, Environmental Sciences School, National University, Heredia 40101, Costa Rica; tomas.soto.murillo@una.ac.cr (T.S.-M.); jose.rojas.marin@una.ac.cr (J.F.R.-M.); victor.beita.guerrero@una.ac.cr (V.H.B.-G.); maria.hidalgo.gutierrez@una.ac.cr (M.H.-G.)

* Correspondence: jorge.herrera.murillo@una.ac.cr; Tel.: +506-2277-3292

Abstract: The concentrations of water-soluble anions present in PM₁₀ collected from ambient air in four sites of Costa Rica's greater metropolitan area (GAM) were analyzed. Samples were collected over a 24-h period for three days during the 2011–2018 period, using high-volume air samplers with mass flow controller. The PM₁₀ samples were collected using quartz fiber filters, which were analyzed using ion chromatography to identify organic and inorganic ions. The annual averages for PM₁₀, F⁻, Cl⁻, and SO₄²⁻ showed significant differences between the sampling sites, with Uruca (UR) consistently registering annual averages above the maximum concentration established by Costa Rica's air quality regulations (30 µg m⁻³). The ions analyzed contributed 33%, 34%, 35%, and 37% of the PM₁₀ mass for sampling sites UR, HA, AL, and CA, respectively. Using Spearman correlations and principal component analysis (PCA), the following contributions were identified: biomass burning, secondary particle formation processes from mobile and stationary emissions, and biogenic emissions. For each variable, seasonal patterns and trends were analyzed using time series with additive decomposition.

Keywords: source apportionment; time series; Costa Rica; air quality



Citation: Herrera-Murillo, J.; Soto-Murillo, T.; Rojas-Marín, J.F.; Beita-Guerrero, V.H.; Hidalgo-Gutiérrez, M. Water-Soluble Anions in PM₁₀ Samples Collected in the Metropolitan Area of Costa Rica: Temporal and Spatial Variations. *Atmosphere* **2021**, *12*, 1264. <https://doi.org/10.3390/atmos12101264>

Academic Editor: Kimitaka Kawamura

Received: 19 August 2021
Accepted: 24 September 2021
Published: 28 September 2021

Publisher's Note: MDPI stays neutral with regard to jurisdictional claims in published maps and institutional affiliations.



Copyright: © 2021 by the authors. Licensee MDPI, Basel, Switzerland. This article is an open access article distributed under the terms and conditions of the Creative Commons Attribution (CC BY) license (<https://creativecommons.org/licenses/by/4.0/>).

1. Introduction

Costa Rica's greater metropolitan area (GMA) is a multinuclear region, comprising the cities of Alajuela, Cartago, Heredia, and San Jose, which function as subcenters, favoring poor-quality public transportation and vial infrastructure exclusively featuring a radial road system that hinders mobility in the region. This geographical area includes 3.83% (2.044 km²) of the total national territory, but houses approximately 60% of the population (2.6 million), representing the most urbanized, populated, and economically active region in the country [1]. Demographic and economic growth patterns and a lack of adequate territorial planning have generated a sustained deterioration of air quality in the GAM, where particles constitute one of the main air pollutants [2].

The World Health Organization (WHO) has indicated that particulate matter (PM) is one of the pollutants that most affects people, with issues such as cardiovascular and respiratory disease resulting from chronic exposure [3–7]. Likewise, recent studies have associated the concentration of PM in urban areas with lung damage and increased mortality [8]. PM₁₀ is considered one of the pollutants with the greatest effect on human health, causing immune system reactions, lung irritation, cell damage, asthma, chronic bronchitis, cancer, and even death [9]. Particulate matter also impacts the environment, generating stress on the ecosystem and promoting its degradation and the loss of sensitive species [10]. The continuous exposure of plants to air pollutants makes them susceptible to their effects. PM tends to deposit on plant leaves, causing acute damage over short

periods when the concentrations are high and generating necrotic lesions. If the exposure is over a broader period under low concentrations of the pollutant, then chronic effects, such as leaf injury, stomatal damage, premature senescence, decreased photosynthetic activity, disturbed membrane permeability, and reduced growth and yield, appear. Likewise, morphological impacts are observed as a decrease in the area and number of leaves due to the obstruction of the stomata caused by the particles, which disrupt the physiological activity of the plant [11]. Particulate matter also reduces photosynthetically active radiation (PAR) by altering the surface optical properties, affecting the photosynthetic activity of the plant and increasing the temperature of the leaves [11,12]. Similarly, the ecosystem's soils are affected by the particulate matter deposition, which alters their chemical composition and pH and results in diverse effects depending on the origin and nature of the particles, among these the reduction of available nutrients in the soil or the introduction of heavy metals into the ecosystem, inhibiting plant growth [13]. The composition of the PM can vary widely depending on the source and the environmental conditions. Among the substances that comprise these particles, studies have detected fatty acids, n-alkanes and iso-alkanes, phthalate esters, siloxanes, sterols, sugars and sugar alcohols, lignin tracer compounds and resin acids, dicarboxylic acids, polycyclic organic compounds, organic nitrogen compounds, and products from secondary oxidation of monoterpenes [14].

The fraction of water-soluble components (WSC) in the particles contain both inorganic ions and organic compounds, which exert an influence on the activity of condensation nuclei of the cloud, the size of the particulate material, and the toxicity [15]. The concentration of ionic inorganic species accounts for approximately one-third of the fine fraction and is mainly influenced by prevailing weather factors, geographical conditions, and the variability of the emission sources [16]. Several studies have shown that secondary inorganic ions (SO_4^{2-} , NO_3^- and NH_4^+) dominate water-soluble ionic species and define the acidic or alkaline nature of the particles [17]. However, there have been few studies aimed at quantifying the presence of water-soluble organic compounds. Thus, monocarboxylic and dicarboxylic acids, for example, are key groups of organic compounds that have been identified in atmospheric particles [18]. Both formic and acetic acid, as well as oxalic acid, have also been detected in samples of particles collected in urban and rural environments [19]. These acids have a high water solubility and the potential to modify the hygroscopic properties of the particles, including their size and the activity of the condensation nuclei [20]. In the particulate phase, most of these acids are neutralized as formate, acetate, and oxalate salts [21], derived mainly as a product of biomass burning or from secondary reactions in the atmosphere [22,23]. Although particulate oxalate is highly hygroscopic, its concentration is much lower when compared to sulfate and nitrate [24]. However, a study on Brazil's urban areas showed that oxalate is the water-soluble organic ion with the highest concentration on PM_{10} particles [25]. The chemical composition of the particles has a significant effect on global weather patterns [26], human health [27], and air quality.

In this study, the temporal and spatial variations of water-soluble anions present in samples of PM_{10} particles collected in the metropolitan area of Costa Rica were analyzed to determine the possible sources that originate them and, thus, guide the actions that must be included in the respective air quality management plans.

2. Materials and Methods

2.1. Sampling

For the PM_{10} sampling, 4 monitoring sites were selected Table 1. The sites were representative of commercial, industrial, and residential areas, all located in Costa Rica's metropolitan area Figure 1.

Sampling campaigns were conducted from January 2011 to December 2018. Twenty-four-hour PM_{10} samples were collected once a day for three days using high-volume air samplers (Hi-Vol) with MFC (mass flow controller), operating at a flow rate of $(1.13 \pm 10\%) \text{ m}^3 \text{ min}^{-1}$

with 10 µm size-selective inlets (Thermo Andersen, Massachusetts, USA). Table 2 summarizes the number of samples collected per year.

Table 1. PM₁₀ sampling sites in the metropolitan area of Costa Rica.

Sites	Type	Coordinates		Height (m)
		Latitude	Longitude	
Hatillo (HA)	Residential	9°55′8.60″ N	84°6′17.80″ W	1114
Uruca (UR)	Industrial–Commercial	9°57′7.24″ N	84°6′24.95″ W	1098
Cartago (CA)	Commercial	9°52′1.38″ N	83°55′19.61″ W	1448
Alajuela (AL)	Commercial–Residential	10°0′28.12″ N	81°13′3.88″ W	904

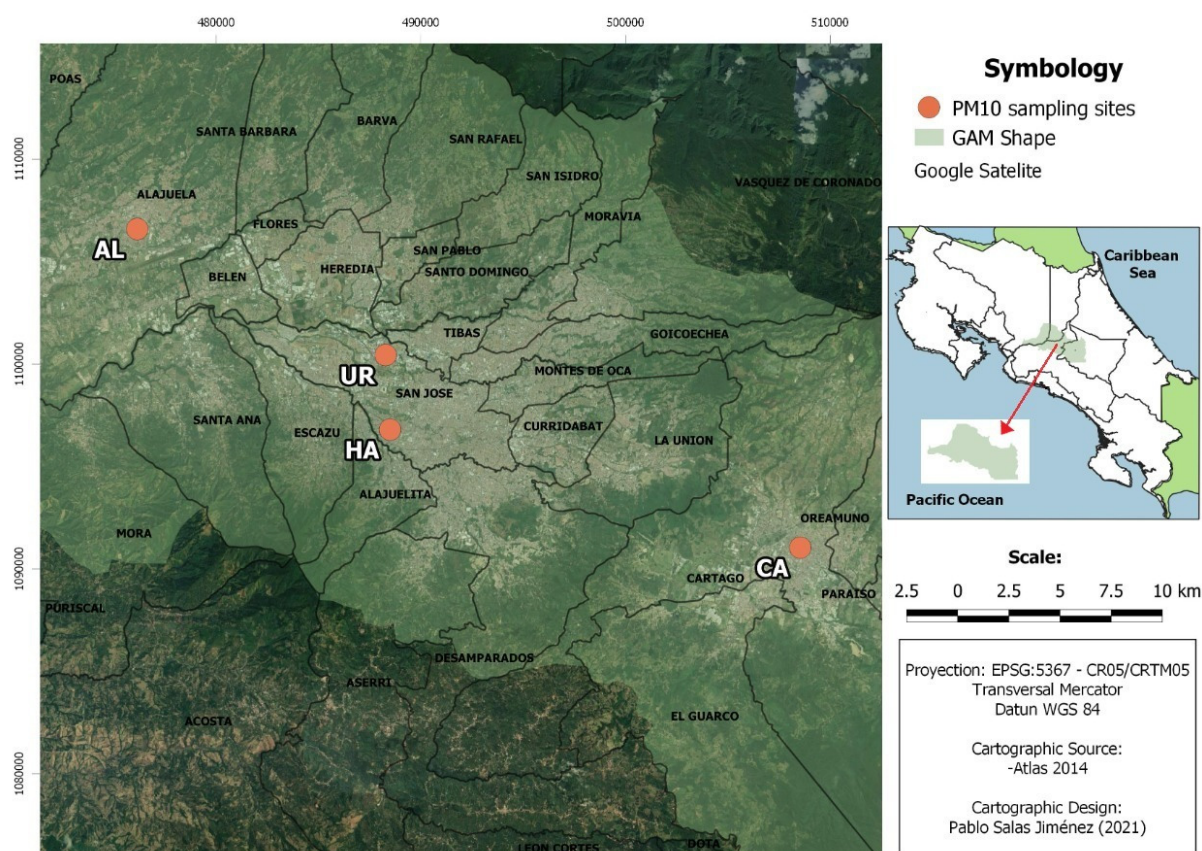


Figure 1. Geographical distribution of the selected monitoring sites of the air quality network from the Costa Rican metropolitan area.

Table 2. Sample distribution for each site, 2011–2018.

Sampling Sites	2011	2012	2013	2014	2015	2016	2017	2018
HA	76	95	106	93	91	110	95	102
UR	100	87	101	98	94	114	101	99
CA	92	109	112	101	108	105	98	97
AL	93	99	103	95	96	102	104	106

Temperature and pressure during the sampling were determined to calculate the actual air volume for each sample under standard conditions (25 °C and 1 atm). Quartz fiber filters (Whatman CAT No. 1851–865, Massachusetts, USA) were used for particle sampling, which were desiccated for 24 h after sampling in a desiccator under the following conditions:

temperature of 15–30 °C and humidity of less than 40%. PM₁₀ mass concentrations were measured gravimetrically by weighing the quartz fiber filters (twice) before (blank filter) and after (total filter) sampling using an analytical balance.

2.2. Filter Extraction

Water soluble ions were extracted from a 2.54 cm by 23 cm strip of each quartz filter used for the gravimetric analysis. The strip was placed in a 150 mL beaker containing 50 mL distilled and deionized water (DDW) (18.2 MΩ resistivity). The beakers were placed in an ultrasonic water bath for 30 min at room temperature. The solution was then poured into a volumetric flask and filled to the mark with DDW. The extracts were filtered through 0.45 μm pore-size microporous membranes before instrumental analysis.

2.3. Chemical Analysis

A water-soluble anions analysis was performed by dual-microbore-suppressed ion chromatography using a DIONEX ICS-3000 machine with a quaternary pump. For the anion analyses, the instrument was equipped with an IonPac AS14A column (8 mM Na₂CO₃/1 mM NaHCO₃ as the eluent). Ionic species were identified and quantified by interpolation on a calibration curve of 7 standard solutions and were prepared from certified commercial solutions (MERCK Suprapur solutions, Hong Kong, China). A fresh calibration curve was prepared for every 20 samples, together with a dissolution of quality control of 5 mgL⁻¹ prepared from a certified DIONEX synthetic sample. Detection limits for each ion are shown in Table 3.

Table 3. Detection limits for the analyzed ions in PM₁₀.

Ion Specie	Detection Limits (μgm ⁻³)
Fluoride (F ⁻)	0.01
Formate (HCOO ⁻)	0.01
Acetate (CH ₃ COO ⁻)	0.03
Chloride (Cl ⁻)	0.02
Nitrite (NO ₂ ⁻)	0.02
Nitrate (NO ₃ ⁻)	0.02
Phosphate (PO ₄ ³⁻)	0.03
Sulfate (SO ₄ ²⁻)	0.03
Oxalate (C ₂ O ₄ ²⁻)	0.02

2.4. Statistical Analysis

The statistical analysis was conducted using Minitab software. First, an Anderson–Darling normality test was used to compare the empirical cumulative distribution function of the sample data with the expected distribution function as if the data were normal, wherein a large enough difference (a *p*-value less than the significance value) rejects the null hypothesis [28]. An analysis of variance (ANOVA) was then conducted. As this study contained several datasets, each with a significant number of factors, the ANOVA was used even when these showed abnormal behavior, as this parametric test provides a higher resolution than non-parametric methods and is effective with a large enough sample size [29]. The ANOVA was used to compare the mean value of the ions per sampling site and year. While the test can evidence statistically significant differences between two or more levels of a given factor, it does not specify between which factors these differences were observed [30]. Thus, Tukey’s method of multiple comparisons was used in conjunction with the ANOVA to create confidence intervals between each pair of differences analyzed, enabling us to specify between which levels the differences shown in the ANOVA were observed [29]. Additionally, a Spearman correlation test was used to verify the correlation between two

variables when the relation between them was nonlinear, measuring the monotonic relationship between two continuous or ordinal variables. In this case, the p -value indicated the statistical significance of the correlation, while the Spearman coefficient indicated its strength [31]. Lastly, a principal component analysis (PCA) was conducted. This technique helps decrease the dimensionality of the variables by using the correlations or levels of association between them to classify a large number of variables based on their correlational proximity. This method consists of obtaining the main components, scaled for one of the sample sights, and taking from these only those components with a variance of greater than 1, allowing the groupings to be observed graphically. All data were processed using the R Core Team (2020).

2.5. Time Series

To analyze the temporal variation of the parameters measured (trends and seasonal patterns), respective time series were constructed, for which the information needed to be divided in a uniform manner. For this, an average monthly observed concentration was obtained for PM_{10} , F^- , Cl^- , NO_3^- , and SO_4^{2-} from January 2011 through December 2018, leading to a series of 96 datasets for each variable and sampling site. The remaining results, which pertained to a statistically insignificant portion of the total, were replaced through linear interpolation, considering the anterior and posterior values. This process did not affect the trend analysis for each time series. Once the database was refined, obtaining a single (average) monthly value, we proceeded to generate a time series for each variable per sampling site. All data were processed using the R Core Team (2020). As such, charts corresponding to the series were generated, as well as those of their respective decompositions into their various components.

The Mann–Kendall trend statistical test was applied to account for enough evidence in the significance determination of the trend (consistently increasing or decreasing, $p < 0.05$). A p -value higher than 0.05 does not necessarily imply a nonexistent trend in the longitudinal analysis; instead, it means a not significant result in statistical terms.

3. Results and Discussion

3.1. Concentrations of Water-Soluble Ions and PM_{10}

Table 4 shows the averages and the standard deviations of the data of concentrations of PM_{10} and water-soluble anions obtained for the four sampling sites during the 2011–2018 period.

An Anderson–Darling normality test was performed for each of the parameters evaluated on each collecting site during the sampling period, showing that most of the parameters followed a non-normal distribution.

Upon conducting the variance analysis for the sampling sites, significant differences were found in at least one mean value for PM_{10} , F^- , Cl^- , and SO_4^{2-} , with a significance level of 5%. The average values for the remaining parameters showed no significant differences between the sites. Figure 2 shows the results of the Tukey test, displaying significant differences between the following sites: UR–AL (PM_{10} , F^- , Cl^- , SO_4^{2-}), HA–CA (PM_{10} , F^- , SO_4^{2-}), UR–CA (PM_{10} , F^- , SO_4^{2-}), UR–HA (PM_{10} , SO_4^{2-}), CA–AL (Cl^- , SO_4^{2-}), and HA–AL (Cl^- , SO_4^{2-}). The UR site consistently registered annual averages above the maximum concentration of PM_{10} established by Costa Rica’s air quality regulations ($30 \mu g m^{-3}$). This zone features a high concentration of industrial and commercial activities combined with an increased circulation of light vehicles and heavy cargo and combustion processes from point sources. Differences between AL and all other sites were also found. This site is located downwind from the metropolitan area and is dominated by commercial activities, though with a lower concentration of manufacturing industries. Sampling site HA is also different, as it is the only site located in a residential zone, and it is near an important high-traffic road.

Table 4. Annual average concentrations of PM₁₀ and water-soluble ions (µg m⁻³) and their standard deviations for the 4 sampling sites, 2011–2018.

Year	2011	2012	2013	2014	2015	2016	2017	2018	2011	2012	2013	2014	2015	2016	2017	2018
	PM ₁₀								F ⁻							
HA	34 (19)	27 (7)	28 (9)	26 (7)	25 (6)	26 (9)	26 (8)	25 (7)	0.25 (0.11)	0.31 (0.13)	0.29 (0.08)	0.18 (0.05)	0.24 (0.07)	0.20 (0.08)	0.19 (0.07)	0.21 (0.08)
UR	32 (11)	29 (8)	31 (9)	30 (9)	32 (9)	31 (8)	32 (11)	31 (9)	0.18 (0.16)	0.30 (0.11)	0.27 (0.09)	0.22 (0.06)	0.21 (0.07)	0.16 (0.09)	0.23 (0.07)	0.17 (0.08)
CA	29 (10)	25 (8)	26 (9)	26 (6)	25 (6)	24 (6)	24 (7)	26 (8)	0.15 (0.09)	0.16 (0.07)	0.25 (0.14)	0.22 (0.06)	0.19 (0.08)	0.21 (0.06)	0.15 (0.07)	0.12 (0.08)
AL	27 (6)	22 (6)	27 (10)	26 (6)	28 (9)	25 (6)	25 (5)	23 (4)	0.17 (0.09)	0.20 (0.07)	0.22 (0.06)	0.19 (0.06)	0.19 (0.07)	0.13 (0.05)	0.11 (0.06)	0.12 (0.08)
	HCOO ⁻								CH ₃ COO ⁻							
HA	0.13 (0.07)	0.21 (0.13)	0.26 (0.08)	0.37 (0.11)	0.34 (0.10)	0.29 (0.08)	0.32 (0.09)	0.27 (0.06)	0.17 (0.07)	0.21 (0.08)	0.24 (0.10)	0.20 (0.08)	0.18 (0.09)	0.23 (0.01)	0.25 (0.09)	0.22 (0.07)
UR	0.30 (0.07)	0.33 (0.09)	0.35 (0.12)	0.42 (0.09)	0.40 (0.08)	0.37 (0.06)	0.41 (0.08)	0.34 (0.07)	0.31 (0.08)	0.34 (0.11)	0.50 (0.14)	0.43 (0.07)	0.39 (0.09)	0.44 (0.10)	0.48 (0.12)	0.42 (0.11)
CA	0.65 (0.26)	0.57 (0.32)	0.71 (0.20)	0.70 (0.24)	0.66 (0.15)	0.68 (0.23)	0.59 (0.17)	0.64 (0.27)	0.24 (0.14)	0.26 (0.10)	0.24 (0.15)	0.31 (0.12)	0.28 (0.11)	0.30 (0.16)	0.25 (0.10)	0.27 (0.09)
AL	0.75 (0.34)	0.55 (0.12)	0.87 (0.25)	0.75 (0.31)	0.72 (0.42)	0.66 (0.26)	0.57 (0.31)	0.64 (0.28)	0.57 (0.25)	0.62 (0.18)	0.67 (0.22)	0.70 (0.14)	0.67 (0.27)	0.63 (0.23)	0.55 (0.18)	0.60 (0.14)
	Cl ⁻								NO ₂ ⁻							
HA	1.56 (0.80)	1.33 (0.51)	1.41 (0.43)	1.37 (0.37)	1.78 (0.86)	1.18 (0.53)	1.05 (0.62)	1.14 (0.71)	0.46 (0.21)	0.28 (0.12)	0.42 (0.14)	0.33 (0.17)	0.29 (0.10)	0.36 (0.14)	0.32 (0.18)	0.25 (0.09)
UR	1.36 (0.60)	1.03 (0.35)	1.63 (0.51)	1.46 (0.33)	1.81 (0.81)	1.43 (0.83)	0.98 (0.52)	1.06 (0.62)	0.29 (0.10)	0.26 (0.13)	0.34 (0.10)	0.30 (0.07)	0.26 (0.09)	0.38 (0.11)	0.26 (0.09)	0.38 (0.11)
CA	1.29 (0.73)	1.12 (0.45)	1.84 (0.80)	1.28 (0.34)	1.74 (0.73)	1.56 (0.81)	1.04 (0.67)	1.08 (0.51)	0.19 (0.07)	0.26 (0.10)	0.52 (0.13)	0.43 (0.11)	0.37 (0.08)	0.41 (0.02)	0.29 (0.10)	0.35 (0.09)
AL	1.13 (0.54)	0.94 (0.23)	1.45 (0.40)	1.08 (0.21)	1.68 (0.73)	1.29 (0.96)	0.95 (0.56)	1.01 (0.63)	0.17 (0.06)	0.21 (0.06)	0.25 (0.10)	0.33 (0.09)	0.27 (0.08)	0.34 (0.07)	0.25 (0.07)	0.28 (0.08)
	NO ₃ ⁻								PO ₄ ³⁻							
HA	1.10 (0.32)	0.90 (0.28)	1.20 (0.28)	1.17 (0.24)	1.19 (0.25)	0.93 (0.14)	0.87 (0.22)	0.96 (0.19)	1.46 (0.58)	0.87 (0.38)	0.77 (0.21)	0.95 (0.27)	1.07 (0.34)	0.91 (0.28)	1.14 (0.33)	1.26 (0.35)
UR	0.95 (0.41)	0.92 (0.25)	1.21 (0.36)	1.07 (0.26)	1.28 (0.35)	1.14 (0.43)	0.99 (0.27)	1.07 (0.39)	1.23 (0.37)	1.01 (0.28)	1.08 (0.40)	0.84 (0.27)	1.16 (0.41)	1.04 (0.33)	1.26 (0.53)	1.34 (0.48)
CA	0.66 (0.29)	1.01 (0.40)	1.41 (0.56)	1.33 (0.35)	1.06 (0.36)	1.13 (0.27)	0.94 (0.37)	1.02 (0.28)	1.03 (0.55)	0.70 (0.41)	0.69 (0.38)	0.71 (0.25)	0.88 (0.36)	0.85 (0.32)	0.95 (0.27)	1.01 (0.35)
AL	0.84 (0.33)	0.79 (0.22)	1.16 (0.58)	1.29 (0.37)	0.90 (0.34)	1.06 (0.42)	0.95 (0.38)	0.99 (0.35)	0.84 (0.58)	0.68 (0.37)	0.77 (0.34)	0.81 (0.29)	0.89 (0.33)	0.85 (0.28)	0.91 (0.24)	0.96 (0.37)
	SO ₄ ²⁻								C ₂ O ₄ ²⁻							
HA	4.94 (2.16)	4.43 (1.44)	4.02 (1.77)	3.84 (1.11)	3.70 (1.06)	3.82 (1.37)	3.57 (1.25)	3.89 (1.62)	0.32 (0.07)	0.26 (0.09)	0.22 (0.06)	0.28 (0.08)	0.24 (0.05)	0.30 (0.07)	0.26 (0.08)	0.29 (0.05)
UR	4.51 (2.18)	4.11 (0.92)	4.28 (1.15)	4.10 (1.36)	4.17 (1.06)	4.35 (1.27)	4.13 (0.98)	4.05 (1.05)	0.52 (0.11)	0.47 (0.12)	0.61 (0.24)	0.57 (0.19)	0.64 (0.32)	0.61 (0.26)	0.50 (0.23)	0.55 (0.28)
CA	3.98 (1.68)	3.71 (1.36)	4.01 (1.80)	3.42 (1.28)	3.51 (0.98)	3.45 (1.45)	3.22 (0.75)	3.13 (0.62)	0.27 (0.13)	0.35 (0.12)	0.53 (0.16)	0.41 (0.11)	0.47 (0.15)	0.44 (0.12)	0.36 (0.18)	0.40 (0.10)
AL	4.15 (1.73)	4.03 (1.58)	4.53 (1.36)	3.67 (0.88)	3.75 (0.98)	3.86 (0.81)	3.67 (0.78)	3.57 (0.69)	0.41 (0.01)	0.47 (0.17)	0.52 (0.14)	0.49 (0.21)	0.40 (0.16)	0.44 (0.14)	0.37 (0.12)	0.40 (0.10)

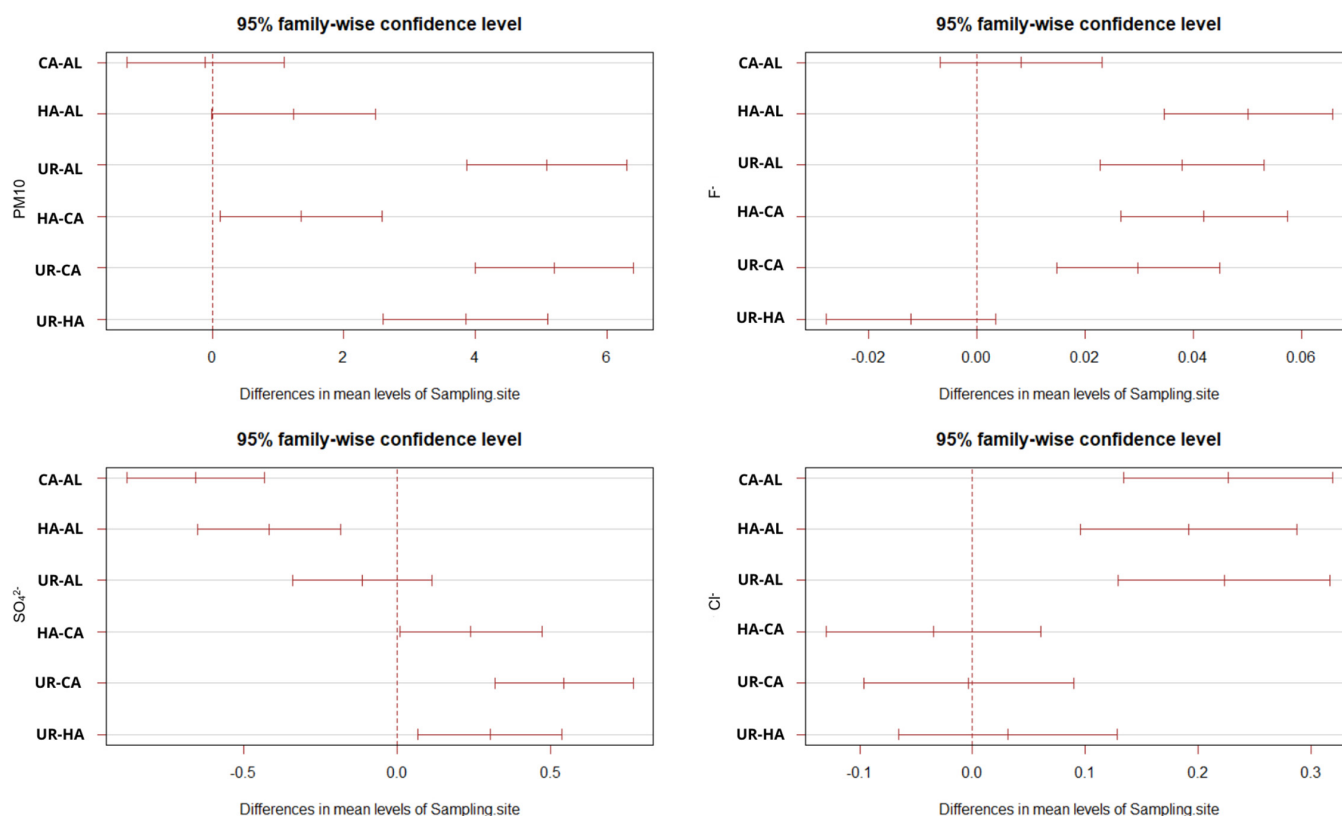


Figure 2. Mean Tukey test results for the sampling sites, 2011–2018.

The ions analyzed contribute to 33%, 34%, 35%, and 37% of the PM_{10} collected for sampling sites UR, HA, AL, and CA, respectively, per the following sequence of individual contribution: $SO_4^{2-} > Cl^- > NO_3^- > PO_4^{3-} > NO_2^- > C_2O_4^{2-} > HCOO^- > F^- > CH_3COO^-$. As shown in Figure 3, the PM_{10} concentrations recorded for the sampling sites during the dry season (December–April) were slightly higher than those recorded during the rainy season (May–November), with some key exceptions. In the dry period, the metropolitan area is influenced by trade winds from the Caribbean Sea, which can have speeds of up to 30 kmh^{-1} and cause a considerable drop in the region’s precipitation levels. For the same reason, recorded concentrations of Cl^- , mainly resulting from the effects of the marine spray, were higher in the dry season. In the case of ions such as nitrate, the formation of which is linked to a transformation from the gaseous to the particle phase, concentrations were higher during the rainy season than the dry season in the majority of cases, possibly because temperatures are lower during this period, while the trade winds that help clear pollutants from the metropolitan area are reduced.

Several authors have used the ion NO_3^- to trace mobile emissions sources through combustion gases created by vehicle exhaust, while SO_4^{2-} indicates emissions from stationary sources. Given this, the relation between the concentration of these ions was used to evidence the influence of mobile emissions as opposed to point sources [32,33]. Figure 4 shows the monthly averages of this relationship throughout the sampling period.

As shown above, the relation between NO_3^- and SO_4^{2-} showed an upward trend for all sampling sites in the 2011–2016 period, while the ratio was more stable in 2016–2018. This could be due to two fundamental variables:

- (1) The sustained growth of the vehicular fleet, as the ratio of vehicles per 1000 inhabitants duplicated between 1994–2014, from 132 to 263 [34];

- (2) A policy recently implemented by the Costa Rican Oil Refinery to make two types of fuel oil available to the industrial market, one of which has a much lower sulfur content than the regular one, which contains around 2% [35].

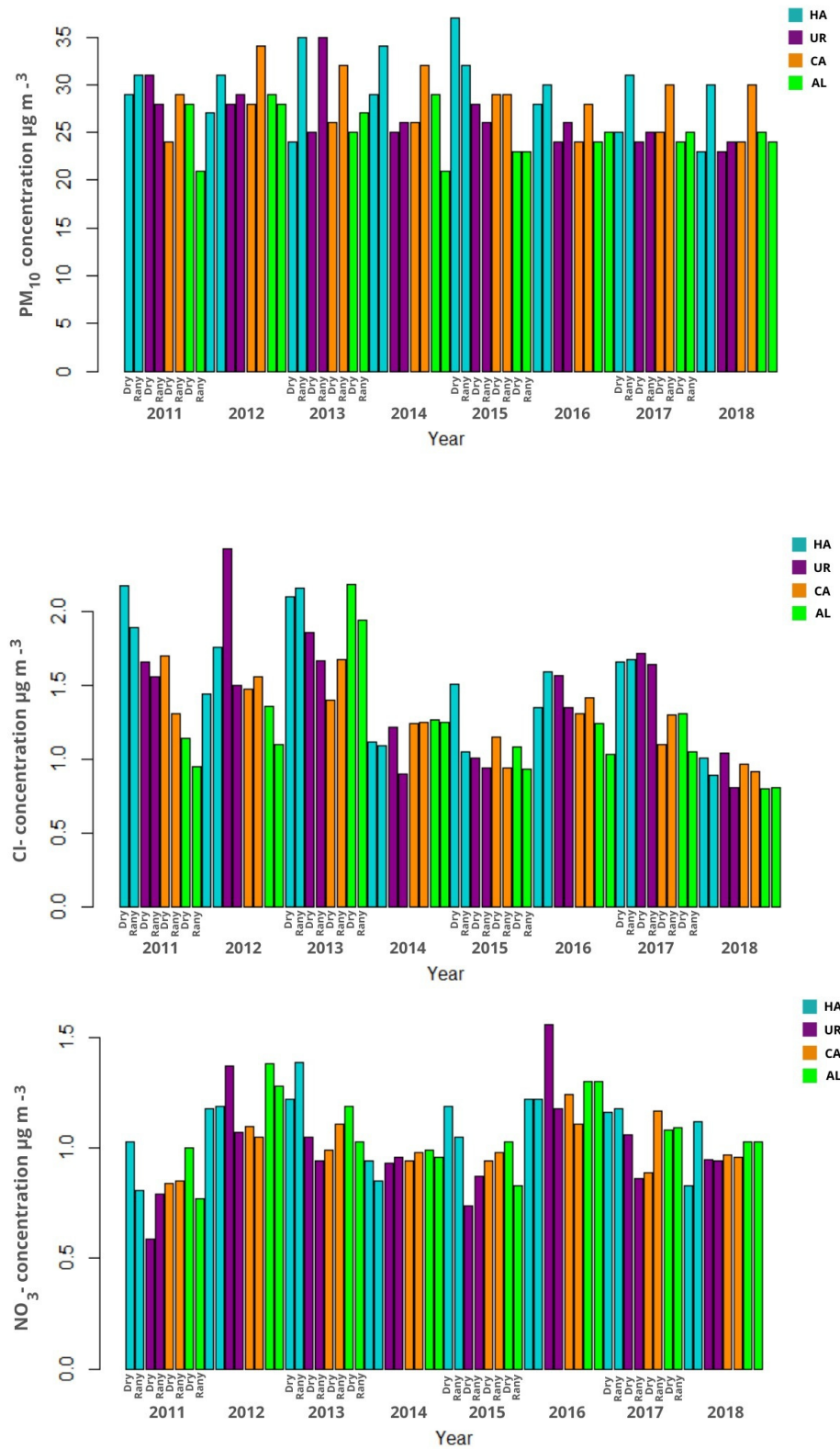


Figure 3. Temporal variations of PM₁₀, Cl⁻, and NO₃⁻ concentration in each sampling site, 2011–2018.

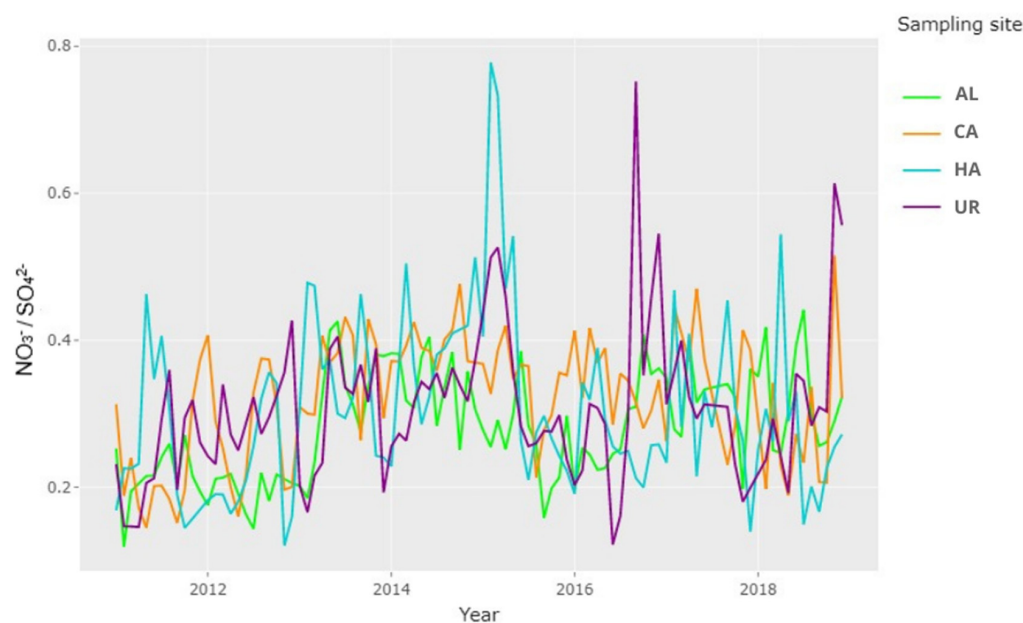


Figure 4. Monthly $\text{NO}_3^- - \text{SO}_4^{2-}$ ratio variation for the sampling sites, 2011–2018.

According to the Mann–Kendall test results, only AL ($p = 0.00002$) and UR ($p = 0.03789$) sites presented a significant statistical trend. But UR and HA exhibited the highest peak ratios, explained by the high vehicular traffic around those areas. It is also relevant to point out that the metropolitan area was affected by emissions from the Turrialba Volcano during the sampling period, presenting significant activity between 2014–2016. However, not the whole time the plume was pointing to the metropolitan area.

3.2. Correlation Patterns between Variables

Table 5 shows the Spearman coefficients for the gravimetric concentrations of PM_{10} , as well as the ions evaluated in the sampling sites. All of these showed a moderate to strong correlation ($\text{HA} = 0.520$, $\text{UR} = 0.577$) between SO_4^{2-} and NO_3^- , which are secondary aerosols that form via the oxidation of SO_2 and NO_x emitted during the burning of fossil fuels. Likewise, a significant correlation between PM_{10} and these ions of secondary origin was identified. For HA, AL, and UR, a moderate correlation was found between $\text{HCOO}^- - \text{CH}_3\text{COO}^-$ (0.396–0.427), $\text{HCOO}^- - \text{NO}_3^-$ (0.351–0.408), $\text{CH}_3\text{COO}^- - \text{NO}_3^-$ (0.422–0.497), and $\text{NO}_2^- - \text{NO}_3^-$ (0.404–0.492), demonstrating the possible influence of secondary formation processes from primary emissions of vehicular sources. For $\text{C}_2\text{O}_4^{2-}$, a moderate correlation was found with NO_2^- for HA, UR, and AL, suggesting a partial apportionment from vehicular emissions and possibly also a contribution from secondary formation through photochemical oxidation of volatile organic compounds. CA was the only site showing a correlation between $\text{C}_2\text{O}_4^{2-}$ and F^- , pointing to the influence of biomass burning emissions. The main sources of HCOO^- , CH_3COO^- , and $\text{C}_2\text{O}_4^{2-}$ in particulate material are primary emissions and the photochemical processes that occur at the atmospheric level. $\text{C}_2\text{O}_4^{2-}$ could originate from oxalic acid in the gaseous phase, which reacts with pre-existing particles via the coagulation of particles or originates from heterogeneous reactions within large droplets [36]. SO_4^{2-} and $\text{C}_2\text{O}_4^{2-}$ did not present significant correlations in all the sampling sites, which could indicate the presence of other primary sulfate sources (e.g., sea salt, combustion, and crustal sulfate), which are as important as secondary formation through in-cloud processing, masking any correlation. Further research is needed for this particular finding.

3.3. Principal Component Analysis (PCA)

Figure 5 shows the results of the PCA obtained for each sampling site. For AL and UR, three factors explained the majority of the data variance. Otherwise, HA and CA required four factors. The first factor presented similar parameters in common for AL, HA, and UR, related to PM_{10} , $HCOO^-$, CH_3COO^- , Cl^- , NO_2^- , NO_3^- , SO_4^{2-} , and $C_2O_4^{2-}$. This suggests that these three sites share the same primary and secondary sources of particulate matter, where combustion emissions are strongly present around the sampling sites. However, for CA, the first factor mainly accounted for F^- , Cl^- , NO_2^- , NO_3^- , SO_4^{2-} , and $C_2O_4^{2-}$, pointing to a significant influence of primary emissions related to fuel burning (mainly biomass). The second factor included PM_{10} , CH_3COO^- , and PO_4^{3-} for most sites, with eigenvalues higher than one. This indicates the influence of particles from biomass burning, except for CA, where PM_{10} , $HCOO^-$, CH_3COO^- , and Cl^- were more important, showing the presence of secondary aerosols from biogenic origin. In all sites, the third factor was more important for F^- , $HCOO^-$, PO_4^{3-} , and $C_2O_4^{2-}$ and related to multiple sources of contribution (mineral dust, biomass burning, fuel emissions).

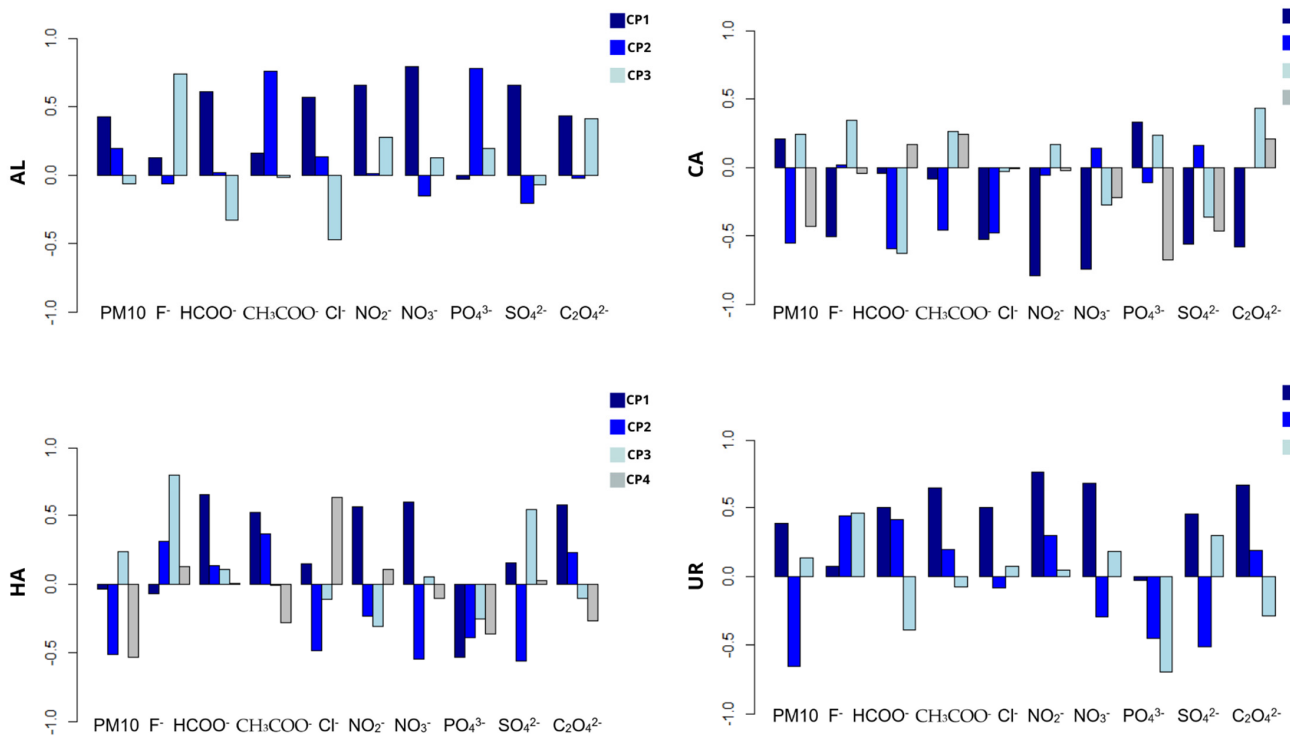


Figure 5. Results of the analysis of the main components of the data for each site.

3.4. Analysis of the Time Series

The behavior of the PM_{10} values and the concentration of the main water-soluble anions through the formulation of time series for each sampling site were analyzed. As shown in Figure 6, all of the parameters evaluated for UR demonstrated well-defined seasonal patterns. For instance, the concentrations of PM_{10} and Cl^- showed higher values during January–April (the dry season) and July, when the rainy season begins to wind down. As explained above, this behavior is partly due to the influence of prevailing winds in the metropolitan area that influence rainfall patterns and are seen as a critical factor in removing atmospheric particulate matter. Additionally, the ions generated through secondary transformation processes, such as NO_3^- , presented a differentiated pattern with higher values during the rainy season due to a drop in temperatures and winds and lessening the chance of contaminant removal.

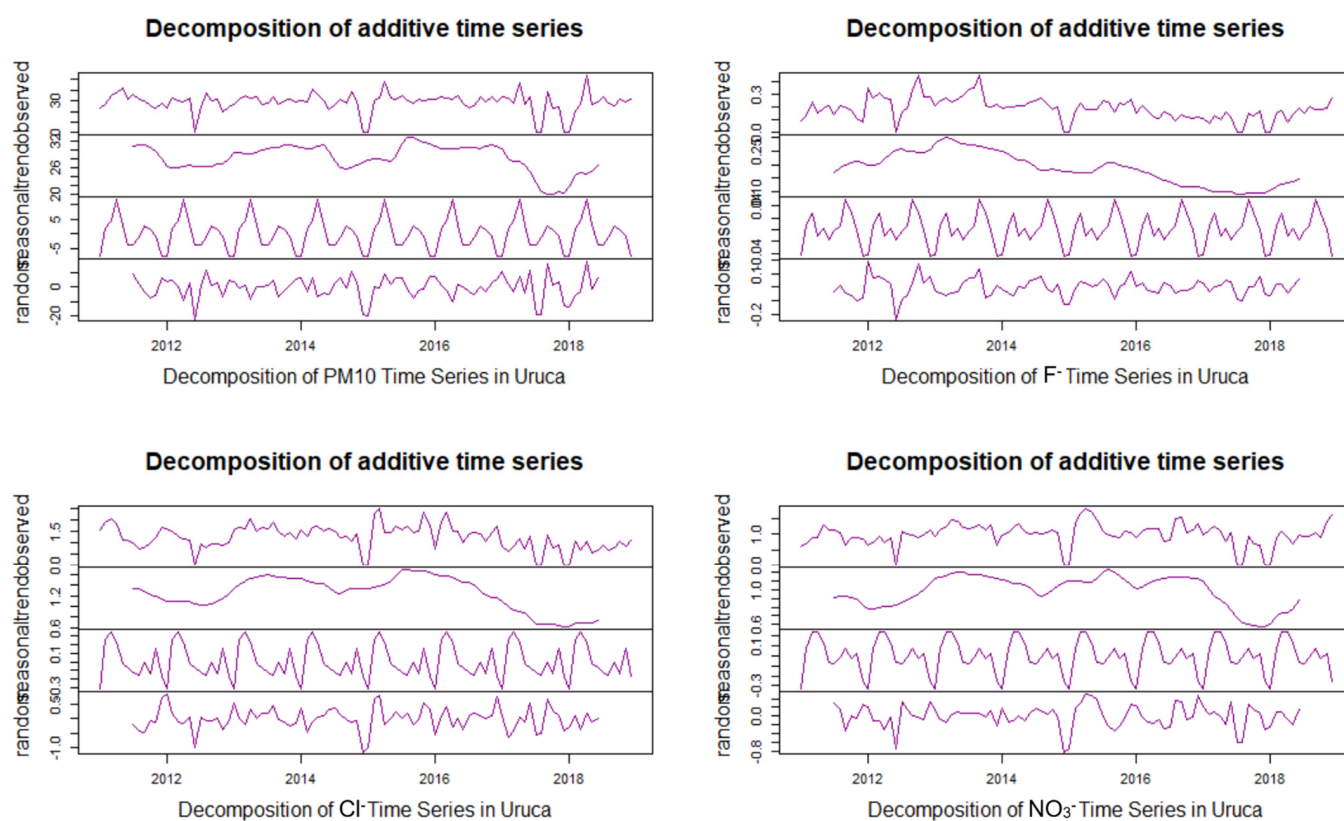


Figure 6. Decomposition of additive time series for the UR sampling site, 2011–2018.

In the case of PM_{10} , as well as for NO_3^- , the data series showed a slight upward trend, possibly attributable to an increase in primary emissions from mobile sources due to a sustained increase in the country's vehicular fleet and a reduction in average circulation speeds throughout its vial infrastructure [2]. F^- showed an inverse behavior, with a sustained downward trend possibly attributable to reduced contributions from biomass burning in this site. The gravimetric concentration of PM_{10} and ions showed similar trends across the four sampling sites studied. According to the results of the Mann–Kendall test, only the trends obtained for F^- ($p = 0.00003$), Cl^- ($p = 0.00145$), and SO_4^{2-} ($p = 0.047$) turned out to be statistically significant.

4. Conclusions

The results obtained from this study suggest that the nature of the processes responsible for PM_{10} generation in the selected sampling sites can vary depending on the predominant land-use patterns in each zone related to the local emissions sources and atmospheric photochemical reactions. UR and AL, which had a significant influence from commercial and industrial activities, showed an important contribution of secondary sources to the particulate matter composition, given the correlations between SO_4^{2-} — NO_3^- , $HCOO^-$ — CH_3COO^- , $HCOO^-$ — NO_3^- , CH_3COO^- — NO_3^- , and $C_2O_4^{2-}$ — NO_2^- , while CA exhibited a stronger correlation for F^- and $C_2O_4^{2-}$, directly related to biomass burning. As for HA, despite being a residential area, it showed a major influence of primary particulate source contributions. The PCA results suggest that AL, HA, and UR sites have the same primary and secondary sources of particulate matter. In contrast, in CA, the primary sources, like biomass burning, seem to be more critical.

The concentrations of anions present in the PM_{10} samples represented between 33 and 37 percent of the total mass collected, with SO_4^{2-} , Cl^- , and NO_3^- being the most abundant elements. As for the organic water-soluble anions, the $HCOO^-$ and CH_3COO^- concentrations were higher in AL, while $C_2O_4^{2-}$ was dominant in UR.

Both the concentration of PM₁₀ and its respective anions presented well-defined seasonal patterns. The PM₁₀ and Cl[−] values, for example, were higher during the dry season than the rainy season due to the influence of trade winds from the Caribbean Sea, which considerably decreased the effect of precipitation as a means of particle removal. NO₃[−], in contrast, showed an inverse behavior, possibly due to higher temperatures during the rainy season combined with a decrease in the removal of pollutants by way of winds.

The relation between NO₃[−] and SO₄^{2−} concentrations showed an upward trend for the 2011–2016 period for all sampling sites, while the ratio between these anions remained stable for 2016–2018. This evidences the influence of a nearly 8% annual increase in the national vehicular fleet in the first case and new policies designed to improve the sulfur content of industrial fuels in the second. UR and HA exhibited the highest peak ratios during the sampling period since both sites are very near high-traffic roads. It can also not be ignored that this ratio was influenced by emissions from natural sources such as volcanic activity.

The low SO₄^{2−} and C₂O₄^{2−} correlations in all the sites suggest that primary sulfate sources could provide a significant contribution to the particulate matter composition, in addition to the well-known secondary formation due to in-cloud processing.

Author Contributions: Conceptualization, J.H.-M.; software and statistical analysis: M.H.-G. and T.S.-M.; data curation: T.S.-M., V.H.B.-G., and J.F.R.-M.; writing—original draft preparation: J.H.-M. and T.S.-M.; writing—review and editing: J.F.R.-M. and V.H.B.-G.; project administration: J.H.-M. All authors have read and agreed to the published version of the manuscript.

Funding: This research received no external funding.

Institutional Review Board Statement: Not applicable.

Informed Consent Statement: Not applicable.

Data Availability Statement: The database is available from the corresponding author upon reasonable request.

Acknowledgments: Not applicable.

Conflicts of Interest: The authors declare no conflict of interest.

References

1. Observatorio urbano del Gran Área Metropolitana (OUGAM). *Datos Estadísticos y Geográficos del Área Metropolitana de Costa Rica*; Universidad de Costa Rica: San José, Costa Rica, 2015.
2. Herrera, J. *Sexto Informe Anual de la Calidad del Aire del Gran Área Metropolitana de Costa Rica*; Universidad Nacional: Heredia, Costa Rica, 2016; pp. 14–29.
3. Li, J.J.; Wang, G.H.; Zhou, B.H.; Cheng, C.L.; Cao, J.J.; Shen, Z.X.; An, Z.S. Chemical composition and size distribution of wintertime aerosols in the atmosphere of Mt.Hua in Central China. *Atmos. Environ.* **2011**, *45*, 1251–1258. [[CrossRef](#)]
4. Norouzi, S.; Khademi, H. Source identification of heavy metals in atmospheric dust using *Platanus orientalis* L. leaves as bioindicator. *Eurasian J. Soil Sci.* **2015**, *4*, 144–219. [[CrossRef](#)]
5. National Pollutant Inventory. *Particle Matter (PM₁₀ and PM_{2.5})*; Australian Government, Department of the Environment and Energy: San José, Costa Rica, 2019.
6. United States Environmental Protection Agency. Particulate Matter (PM) Pollution. 2018. Available online: <https://www.epa.gov/pm-pollution/particulate-matter-pm-basics> (accessed on 5 June 2021).
7. World Health Organization. Ambient (Outdoor) Air Quality and Health. 2018. Available online: [https://www.who.int/news-room/fact-sheets/detail/ambient-\(outdoor\)-air-quality-and-health](https://www.who.int/news-room/fact-sheets/detail/ambient-(outdoor)-air-quality-and-health) (accessed on 6 June 2021).
8. Goudarzi, G.; Geravandi, S.; Mohammadi, M.J.; Vosoughi, M.; Angali, K.A.; Zallaghi, E.; Neisi, A.K.; Saeidimehr, S.; Mohammadi, B. Total number of deaths and respiratory mortality attributed to particulate matter (PM₁₀) in Ahvaz, Iran during 2009. *Int. J. Environ. Health Eng.* **2015**, *4*, 1–7.
9. Khaniabadi, Y.O.; Goudarzi, G.; Daryanoosh, S.M.; Borgini, A.; Tittarelli, A.; De Marco, A. Exposure to PM₁₀, NO₂ and O₃ and impacts on human health. *Environ. Sci. Pol. Res.* **2017**, *24*, 2781–2789. [[CrossRef](#)] [[PubMed](#)]
10. Mohapatra, K.; Biswal, S.K. Effect of particulate matter (PM) on plants, climate, ecosystem and human health. *Int. J. Adv. Technol. Eng. Sci.* **2014**, *2*, 118–129.
11. Rai, P.K. Impacts of particulate matter pollution on plants: Implications for environmental biomonitoring. *Ecotoxicol. Environ. Saf.* **2016**, *129*, 120–136. [[CrossRef](#)]

12. Rahul, J.; Jain, M.K. An investigation into the impact of particulate matter on vegetation along the national highway: A review. *Res. J. Environ. Sci.* **2014**, *7*, 356–372. [CrossRef]
13. Ulrichs, C.; Welke, B.; Mucha-Pelzer, T.; Goswami, A.; Mewis, I. Effect of solid particulate matter deposits on vegetation—A review. *Funct. Plant Sci. Biotechnol.* **2008**, *2*, 56–62.
14. Miuc, A.; Voncina, E.; Lešnik, U. Composition of organic compounds adsorbed on PM₁₀ in the air above Maribor. *Acta Chim. Slov.* **2015**, *62*, 834–848. [CrossRef]
15. Uchiyama, S.; Inaba, Y.; Kunugita, L. Ozone removal in the collection of carbonyl compounds in air. *J. Chromatogr. A* **2012**, *1229*, 293–297. [CrossRef]
16. Satsangi, A.; Pachauri, T.; Singla, V.; Lakhani, A.; Maharaj Kumari, K. Water soluble ion species in atmospheric aerosols: Concentrations and sources at Agra in the indo-Gangetic plain (IGP). *Aerosol Air Qual. Res.* **2013**, *13*, 1877–1889. [CrossRef]
17. Tan, J.; Duan, J.; Zhen, N.; He, K.; Hao, J. Chemical characteristics and source of size-fractionated atmospheric particle in haze episode in Beijing. *Atmos. Res.* **2016**, *167*, 24–33. [CrossRef]
18. Fu, P.; Kawamura, K.; Barrie, L.A. Photochemical and other sources of organic compounds in the Canadian high Arctic aerosol pollution during winter-spring. *Environ. Sci. Technol.* **2009**, *43*, 286–292. [CrossRef] [PubMed]
19. Wang, Y.; Zhuang, G.; Tang, A.; Yuan, H.; Sun, Y.; Chen, S.; Zheng, A. The ion chemistry and the source of PM_{2.5} aerosol in Beijing. *Atmos. Environ.* **2005**, *39*, 3771–3784. [CrossRef]
20. Khan, M.F.; Shirasuna, Y.; Hirano, K.; Masunaga, S. Characterization of PM_{2.5}, PM_{2.5–10} and PM_{>10} in ambient air, Yokohama, Japan. *Atmos. Res.* **2010**, *96*, 159–172. [CrossRef]
21. Kawamura, K.; Bikkina, S. A review of dicarboxylic acids and related compounds in atmospheric aerosols: Molecular distributions, sources, and transformation. *Atmos. Res.* **2016**, *170*, 140–160. [CrossRef]
22. Chianese, E.; Tirimberio, G.; Riccio, A. PM_{2.5} and PM₁₀ in the urban area of Naples: Chemical composition, chemical properties and influence of air masses origin. *J. Atmos. Chem.* **2019**, *76*, 151–169. [CrossRef]
23. Popovicheva, O.B.; Kistler, M.; Kireeva, E.D.; Persiantseva, N.M.; Timofeev, M.A.; Shoniya, N.K.; Kopeikin, V.M. Aerosol composition and microstructure in the smoky atmosphere of Moscow during the August 2010 extreme wildfires. *Izv. Atmos. Ocean. Phys.* **2017**, *53*, 49–57. [CrossRef]
24. Zhou, Y.; Huang, X.H.; Bian, Q.J.; Griffith, S.M.; Louie, P.K.; Yu, J. Sources and atmospheric processes impacting oxalate at a suburban coastal site in Hong Kong: Insights inferred from 1-year hourly measurements. *J. Geophys. Res. Atmos.* **2015**, *120*, 9772–9788. [CrossRef]
25. Souza, D.Z.; Vasconcellos, P.C.; Lee, H.; Aurela, M.; Saarnio, K.; Teinilä, K.; Hillamo, R. Composition of PM_{2.5} and PM₁₀ collected at urban sites in Brazil. *Aerosol Air Qual. Res.* **2014**, *14*, 1–9. [CrossRef]
26. Guo, J.; Liu, H.; Wang, F.; Huang, J.; Xia, F.; Lou, M.; Wu, Y.; Jiang, J.H.; Xie, T.; Zhaxi, Y. Three-dimensional structure of aerosol in China: A perspective from multi-satellite observations. *Atmos. Res.* **2016**, *178*, 580–589. [CrossRef]
27. Chang, C.C.; Lee, I.M.; Tsai, S.S.; Yang, C.Y. Correlation of Asian dust storm events with daily clinic visits for allergic rhinitis in Taipei, Taiwan. *J. Toxicol. Environ. Health-Part A* **2006**, *69*, 229–235. [CrossRef] [PubMed]
28. Pedrosa, I.; Juarros-Basterretxea, J.; Robles-Fernández, A.; Basteiro, J.; García-Cueto, E. Pruebas de bondad de ajuste en distribuciones simétricas, ¿Qué estadístico utilizar? *Univ. Psychol.* **2014**, *14*, 245–254. [CrossRef]
29. Minitab. ¿Qué es el Método de Tukey para Comparaciones Múltiples? Available online: <https://support.minitab.com/es-mx/minitab/18/help-and-how-to/modeling-statistics/anova/supporting-topics/multiple-comparisons/what-is-tukey-s-method/> (accessed on 7 December 2020).
30. Herzog, M.H.; Francis, G.; Clarke, A. ANOVA. In *Understanding Statistics and Experimental Design. Learning Materials in Biosciences*; Springer: Cham, Switzerland, 2019.
31. Roy-García, I.; Rivas-Ruiz, R.; Pérez-Rodríguez, M.; Palacios-Cruz, L. Correlación: No toda correlación implica causalidad. *Rev. Alerg. México* **2019**, *66*, 354–360. [CrossRef] [PubMed]
32. Sharma, M.; Kaskaoutis, G.; Singh, P.; Singh, S. Seasonal variability of atmospheric aerosol parameters over Greater Noida using ground sunphotometer observations. *Aerosol Air Qual. Res.* **2014**, *14*, 608–622. [CrossRef]
33. Kuniyal, J.C.; Sharma, M.; Chand, K.; Mathela, C.S. Water soluble ionic components in particulate matter (PM₁₀) during high pollution episode days at Mohal and Kothi in the North-Western Himalaya, India. *Aerosol Air Qual. Res.* **2015**, *15*, 529–543. [CrossRef]
34. Ministerio de Ambiente y Energía. *VII Plan Nacional de Energía 2015–2030*; Programa de las Naciones Unidas para el Desarrollo: San José, Costa Rica, 2015.
35. RECOPE. *Manual de Productos*; Refinadora Costarricense de Petróleo: San José, Costa Rica, 2019.
36. Wang, Y.; Zhuang, G.; Chen, S.; An, Z.; Zheng, A. Characteristics and sources of formic, acetic and oxalic acids in PM_{2.5} and PM₁₀ aerosols in Beijing, China. *Atmos. Res.* **2007**, *84*, 169–181. [CrossRef]